DEBURRING OF CROSS-DRILLED HOLE INTERSECTIONS BY MECHANIZED CUTTING

Avila, M. C., Choi, J., Dornfeld, D. A.

Laboratory for Manufacturing Automation
University of California, Berkeley
Berkeley, California, United States
mcavila, dornfeld@me.berkeley.edu
jihong@lma.berkeley.edu

Kapgan, M., Kosarchuk, R.

JWDone Company
Hayward, California, United States
mkapgan, kosarchuk@jwdone.com

ABSTRACT

Removal of burrs at cross-drilled hole intersections is often tedious and expensive due to limited accessibility. Automated edge finishing of crossholes has been practiced successfully using robot-assisted, flexible abrasive brush deburring, and non-traditional, mass finishing methods such as electrochemical deburring (ECD), abrasive slurry, and thermal deburring. These methods are very efficient but most require specialized equipment and dedicated cleaning operations to remove chemicals or trapped brush bristles. The Orbitool is an on-line, localized deburring alternative to brushes recently developed by JWDone Company. The Orbitool is a mechanized cutting tool with carbide edges specifically designed for crosshole deburring. Mechanized cutting provides greater selectivity and control of dimensional specifications compared to brushing and mass finishing methods. Furthermore, it can be implemented using existing machine tool equipment and cleaning procedures. As with any deburring tool, its desired capability is burr removal in the shortest time possible while meeting dimensional and surface quality requirements. To this end, process maps of chamfer width and surface roughness of the deburred edges, plotted against process parameters, were developed in this study. Workpieces consisted of Al 6061 T6 bars with zero-offset, perpendicular cross-holes with a diameter of 7.94 mm (5/16 in.). The experiments were conducted using Orbitools with a diameter of 6.35 mm (1/4 in.) and 36 cutting edges. The effect of the process inputs and their mutual interaction was assessed using Taguchi methods. The results show that proper selection of process parameters yield consistent and effective removal of burrs at cross-drilled intersections while achieving surface roughness values that range from 15 to 65 μm at the chamfers.

Keywords: aluminum, bore, burr, chamfering, deburring, drilling, edge finishing, intersecting hole, Orbitool.

INTRODUCTION

Burrs are defined as undesired projections of material beyond the theoretical edges of a machined component due to plastic deformation. Burrs at cross-drilled intersections are frequently found in the production of automotive engine and transmission components. Burrs may affect dimensional tolerances, cause misalignments, and reduce the efficiency and service life of a

component. In many applications, cross-drilled holes act as conduits for lubrication and cooling fluids. Burrs may cause blockage of critical passages and turbulence in the flow of liquids or gases through the conduits, which might cause serious problems during service. Therefore, the development of effective deburring techniques for cross-drilled applications is of great interest in industry.

Gillespie (1975) has indicated that as much as 30% of the manufacturing costs of precision components are incurred by edge finishing. Currently, despite the high degree of automation accomplished in general machining processes, edge finishing of cross-hole intersections is tedious and may entail hand deburring techniques using dental instruments (Gillespie, 1975, 1990). The limited accessibility and relatively complex geometry of hole intersections perplex automation of the deburring stages, and quite often they become bottlenecks in advanced manufacturing systems.

Traditional deburring methods can be classified into global, or mass, methods, and local methods (Dornfeld and Lisiewicz, 1992). Typical global methods include: vibratory deburring, ultrasonic deburring, tumbling, electrochemical deburring, sand blasting, abrasive flow, and brushing (Gillespie, 1975, 1990; Fistere, 1985; Koelsch, 1990). Global methods are very efficient, but edge geometry and surface quality are quite difficult to control. They may also contaminate the parts with chemical or abrasive residues. Broken bristles that get trapped in small holes are often seen while using tube brushes. These shortcomings make difficult subsequent cleaning operations and add expense. Furthermore, with the exception of brushing, which is flexible and fairly simple to automate, global methods generally involve specialized equipment, big capital investments, and "off-line" operation. In contrast, local deburring methods are a selective means of removing the burrs because the point of application of the tools can be controlled. The most common local processes include hand deburring and mechanized cutting. Despite several efforts to automate local deburring operations using feedback control and mechanized cutting (see, for example Gillespie, 1990, Dornfeld and Lisiewicz, 1992), hand deburring is still relied upon when good consistency and tight tolerances are required on surfaces with complex geometries and difficult accessibility such as hole intersections. Surprisingly, very little work has focused on deburring of crossholes (Ohshima et al., 1993, using ball burnishing techniques). To the best of the authors' knowledge, no dedicated work has been carried out in the study of local, mechanized cutting deburring methods intended for cross-drilled hole intersections.

Recently, JWDone company developed the "Orbitool" a local deburring tool specially designed for cross-drilled hole intersections. It is intended for machine tool usage in on-line configurations. In this study, a full factorial design of experiments was applied to determine the effect of process parameters on chamfer size and surface roughness of the deburred edges. Sensitivity analysis using Taguchi methods was performed to asses the effect of input parameters on chamfer size and their mutual interaction.

THE ORBITOOL

The Orbitool is a mechanized cutting deburring tool designed to selectively create a chamfer on the edges of cross-drilled hole intersections, and remove the burrs formed therein, while causing virtually no damage to the surfaces of the holes. It consists of the following parts: (1) semi-spherical carbide cutter, (2) polished steel protective disk, (3) tool-steel shaft, (4) elastomer flexible coupling, and (5) drive shaft (Figure 1).

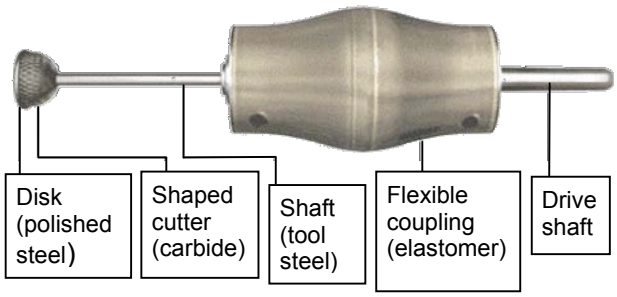

FIGURE 1. THE ORBITOOL AND ITS COMPONENTS.

Figure 2 depicts the standard tool path of the Orbitool. To perform the deburring operation, the tool is first inserted into the smallest diameter hole of the intersection, following the axis of the

hole, and positioned in such a way that the tip of the tool is as close as possible to the intersection (a). Then, the tool is moved towards the surface of the hole, until the axis of the tool coincides with the diameter of interpolation (b). The resultant load between the tool and the workpiece is a function of the stiffness of both the elastomeric coupling and the tool shaft. At this stage, only the protective disk is making contact with the surface of the hole. The tool is then spun on its own axis and interpolated following a helical path, inward into the hole (c). As the tip of the tool reaches the intersection, the carbide cutter makes contact with the edge and the cutting process begins. Once the entire profile of the cutter has traversed the intersection (d), the tool is stopped, brought back to the centerline of the hole, and withdrawn (e).

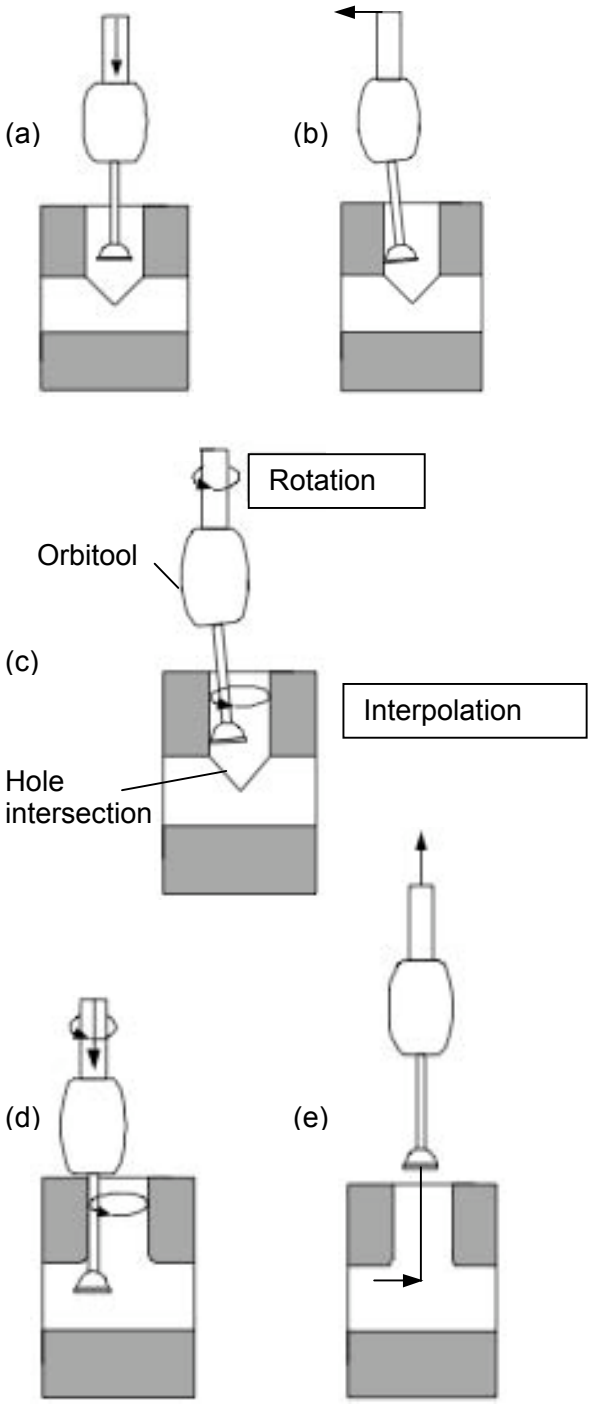

FIGURE 2. OVERWIEW OF THE ORBITOOL PATH. (a) INSERTION INTO HOLE, (b) LOADING, (c) START OF MACHINING, ROTATION AND INTERPOLATION, (d) END OF MACHINING (e) WITHDRAWAL.

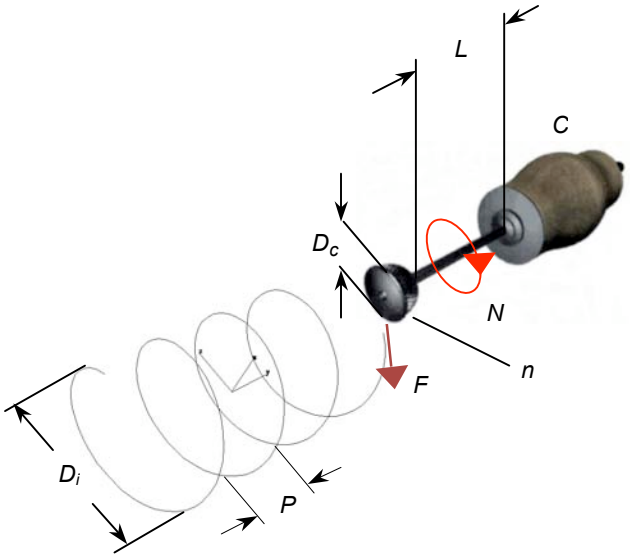

FIGURE 3. ORBITOOL DEBURRING PROCESS PARAMETERS. D_i: DIAMETER OF HELICAL INTERPOLATION, P: HELICAL PITCH, L: SHAFT LENGTH, C: COUPLING TYPE, D_c: CUTTER DIAMETER, n: FLUTE COUNT, N: SPINDLE SPEED, F: FEEDRATE.

TOOLPATH AND DEBURRING PROCESS PARAMETERS

Figure 3 presents a schematic view of process parameters and toolpath of the deburring process. The standard Orbitool toolpath consists of a helix, with respect to a frame of reference on the workpiece. The helical interpolation is defined by the diameter of interpolation D_i and the helical pitch P. D_i depends on the geometry of both the workpiece and the tool, namely:

$$D_i = D - D_s - \delta \quad (1)$$

where D is the diameter of the hole, D_s the diameter of the tool shaft, and δ a diametrical clearance intended to reduce rubbing between the shaft and the workpiece (Figure 4). P defines the number of tool passes along the intersection. Small P values increase tool dwell and material removal rate. The length of the tool shaft L and the diameter of the cutter D_c also depend on the geometry of the workpiece. L affects the bending stiffness of the cutter, and should be adjusted so that the entire profile of the cutter is capable of reaching the burr-prone areas of the cross-hole intersection. However, L should be set as short as possible to prevent excessive tool runout. On the other hand, the size of the cutter should be small enough to fit into the hole and interpolate freely, but large enough to maximize effective cutting speed and material removal rate. n denotes the number of flutes in the cutter. A coarse flute count yields better efficiency but lower surface quality compared to a fine flute count. C represents the type of flexible joint, which is characterized by its bending stiffness and its mass. C affects the cutting loads and material removal rate. Kinematical parameters of the deburring process are translational (interpolation) speed or feedrate F and rotational speed N.

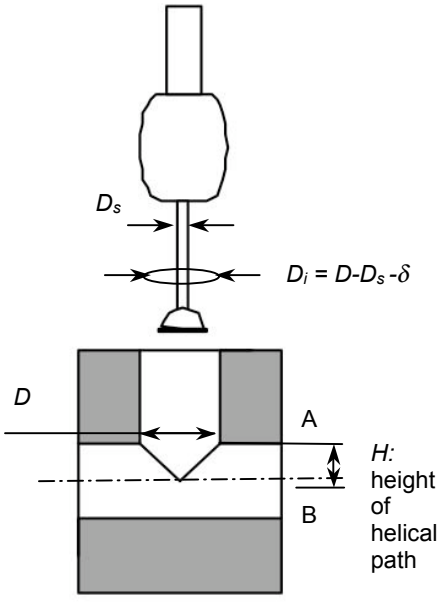

FIGURE 4. SCHEMATIC VIEW OF INTERSECTING HOLE DIAMETER (D), DIAMETER OF INTERPOLATION (Di), AND HEIGHT OF HELICAL PATH (H).

The duration of a deburring operation, denoted t, depends on the length of the helical toolpath, and the speed of interpolation along the path. The length of the path depends on the diameter of interpolation, helical pitch, and height of helical path H. Cycle time is calculated from the following expression:

$$t = \frac{H}{PF}\sqrt{(P^2 + \pi^2 D_i^2)} \quad (2)$$

SELECTION OF PROCESS PARAMETERS FOR OPTIMAL DEBURRING

Special care should be practiced in the selection of deburring process parameters, in order to assure thorough burr removal, that dimensional tolerances are met, and to satisfy surface quality requirements. For example, excessive dwelling or too slow feedrate can lead to undue chamfering of the edges. Likewise, insufficient dwelling or too slow rotational speed may not remove the burrs at all. In most instances, it is desirable to machine off the least amount of material necessary to completely, and consistently, remove the burrs. Evidently, the optimum chamfer size or material removal is subject to the dimensions of the burrs, specifically, their root thickness. Hence, to minimize chamfering during the deburring stage, prior drilling processes must yield limited and repeatable burr sizes.

Process maps showing the dependence of chamfer size and surface quality on input parameters allow the process engineer to select the appropriate set of conditions, based on design specifications and burr root thicknesses formed during upstream drilling operations. In this study, chamfer size and surface roughness charts were developed, specifically for deburring of Al 6061-T6 using an Orbitool with a semi-spherical carbide cutter of 6.35 mm (1/4 in.) in diameter and with 36 cutting edges.

Cycle time constraints are also critical during the selection of process parameters. It is desirable to minimize H so that no time is spared during the deburring cycle. To this end, the tip or disc of the Orbitool shall be placed by rapid-move directly above the intersection, point A, as shown in Figure 4. Additionally, the deburring path can be finalized before the profile of the carbide traverses the entire intersection, at point

B, because burrs may not exist beyond certain regions due to the increase in exit angle. The cycle time abacus shown in Figure 5, which stems from Equation (2), provides a useful means of estimated deburring times given H, P, D_i , and F.

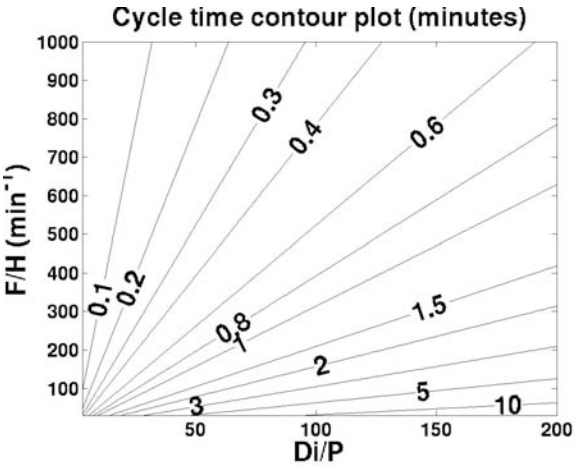

FIGURE 5. CYCLE TIME CONTOUR PLOT AS A FUNCTION OF F, P, D_i, AND H.

EXPERIMENTAL FRAMEWORK

A full factorial experiment design was used initially to investigate the mechanized, local deburring process of intersecting holes using the Orbitool. A full factorial scheme was justified by the unknown response of output parameters from the Orbitool deburring technique. The goal of the experiments was to assess the effect of process input factors on chamfer size and surface roughness. The controllable input factors varied were: flexible coupling type (C), tool shaft length (L), helical pitch (P), feedrate (F) and spindle speed (N). On the other hand, the diameter (D_c), and number of flutes of the cutter (n), were fixed throughout the experiments. Table 1 shows the test matrix with control factors and corresponding levels.

Test samples were manufactured from Al 6061-T6 bars. 22 cross-holes were drilled in each sample (Figure 6). The geometric characteristics of the hole intersections are indicated in Table 2.

The deburring experiments were performed using a Matsuura MC-510V CNC vertical machining center. Dry cutting was chosen because the Orbitool deburring process generally involves low material removal rates and low heat generation. Each combination of factors was executed twice to assure statistical significance.

TABLE 1. CONTROL FACTORS OF FULL-FACTORIAL EXPERIMENT DESIGN.

Factors	Levels	
Cutting tool diameter (D_c)	Dc = 6.35 mm (1/4 in.)	
Number of cutting edges (n)	n = 36	
Coupling type (C)	C1	Stiffness: 1.8 N · m/ deg
		Mass: 34.12 g
	C2	Stiffness: 3.2 N · m/ deg
		Mass: 63.02 g
Shaft length (L) (mm)	L1 = 51 (2.0 in.)	
	L2 = 102 (4.0 in.)	
Helical Pitch (P) (mm)	P1 = 0.05 (0.002 in.)	
	P2 = 0.36 (0.014 in.)	
	P3 = 0.66 (0.026 in.)	
	P4 = 0.96 (0.038 in.)	
	P5 = 1.27 (0.050 in.)	
Feedrate (F) (m/min)	F1 = 0.33 (13 in./min)	
	F2 = 2.7 (106 in./min)	
	F3 = 5.0 (198 in./min)	
Spindle Speed (N) (rpm)	N1 = 2000	
	N2 = 4000	
	N3 = 6000	
	N4 = 8000	

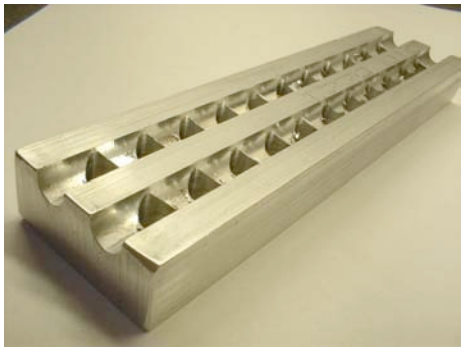

FIGURE 6. Al 6061-T6 TEST SAMPLE.

TABLE 2. GEOMETRIC CHARACTERISTICS OF HOLE INTERSECTIONS.

Geometric characteristic	Value
Hole diameter	7.94 mm (5/16 in.)
Cross-hole to intersecting hole diameter ratio	1
Angle of intersection	90°
Offset distance	0.0 mm (0.00 in.)

The projected width of the chamfers *Wc* was selected as a metric of chamfer size in order to simplify measurement. The projected width was measured by means of an optical coordinate measuring machine. Measurements were taken at the diametrically opposed points were the angle of the edges in the meridional view is equal to 90°; both valued were averaged. At these points, the exit angle of the drill is 90°. With the geometric characteristics shown in Table 2, 90° is the minimum exit angle along the intersection, and maximum burr formation takes place at these points. This is explained by the fact that burr size increases monotonically with decreasing exit angle (Kim et al., 1999). For successful deburring, the amount of chamfering must be at least equal to the root thickness of the largest burrs along the intersection. Hence, measurements of chamfer width were taken at the aforementioned points. Contour process maps were developed by plotting the *Wc* data against the control factors. In addition, to better understand the effect of each of the control factors on *Wc* and their mutual interaction, and to distinguish the factors that have the strongest and weakest effects on process output, marginal mean graphs were plotted using Taguchi robust design methods. An L_{16} orthogonal array (2^5 fractional factorial design with resolution V) was chosen to perform the analysis.

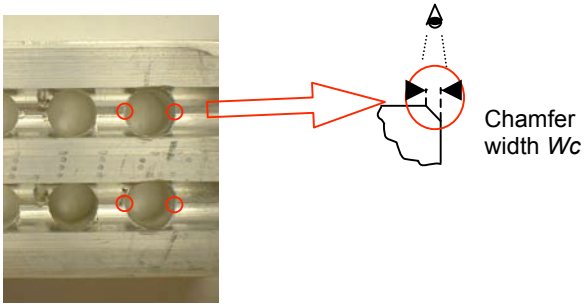

FIGURE 7. PROJECTED SIZE OF CHAMFER.

Surface roughness was gauged on the edges corresponding to L1 and C2 conditions only. R_a and R_t roughness values were measured using a Veeco optical interferometer. Sampling beams were focused on one of the 90° exit angle areas of the intersections. Within each sampling window, 3 profiles perpendicular to the tool marks were recorded and their R_a and R_t roughness values averaged. Replication was not exercised in the roughness measurements because good repeatability was observed.

RESULTS AND DISCUSSION

Figures 8, 9 and 10 show contour plots of chamfer size as a function of spindle speed and helical pitch, using feedrates F1, F2, and F3, respectively. The graphs correspond to the L2-C2 condition (long shaft, stiff coupling). A number of significant features can be discussed about the behavior of the Orbitool deburring process. First, one key result is the monotonic response of *Wc* vs. *P* and *N*. Chamfering increases with increasing rotational speed and with decreasing helical pitch. This same behavior was seen throughout all testing conditions. Second, the increase in chamfer width as rotational speed increases becomes less important as N approaches 8000 rpm. This behavior suggests that dynamic effects of the tool's rotating mass above 8000 rpm may reduce chamfering efficiency. Third, a

comparison between the three graphs illustrates that material removal decreases with increasing feedrate. It is worth noting, however, that the decrease in chamfer width becomes modest as the feedrate is varied from F2 to F3. This result is quite advantageous, as faster cycle times can be realized while incurring low reduction in chamfering efficiency. Likewise, the 2 latter results were evidenced across all testing conditions.

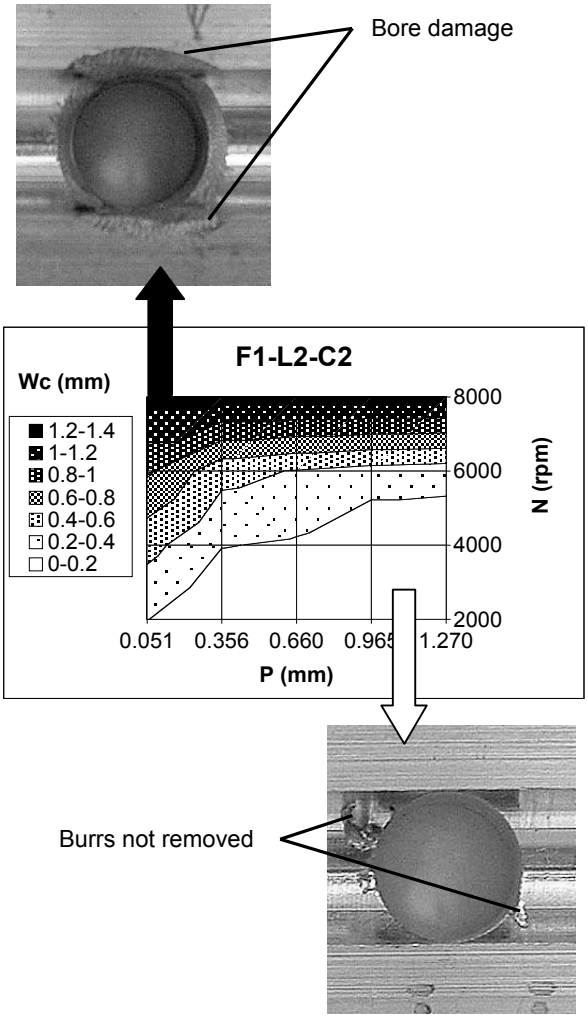

FIGURE 8. PROJECTED CHAMFER WIDTH *Wc* AS A FUNCTION OF HELICAL PITCH (*P)* AND SPINDLE SPEED (*N)*. INTERPOLATION SPEED (F1) = 0.33 m/min, SHAFT LENGTH (L2) = 102 mm, C= C2. ALSO SHOWN: TOP-VIEW PHOTOGRAPHS OF HOLE INTERSECTION WITH EXCESSIVE OVERCUT (TOP) AND INSUFICIENT CHAMFERING FOR BURR REMOVAL (BOTTOM).

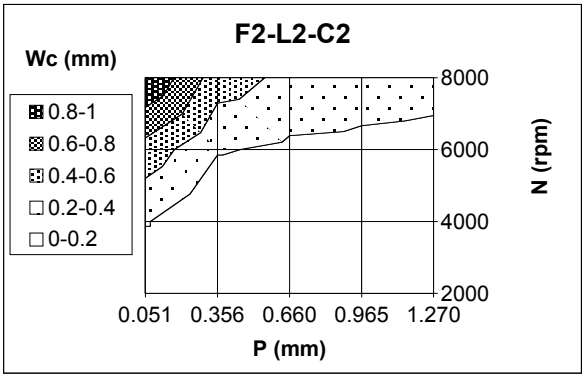

FIGURE 9. PROJECTED CHAMFER WIDTH *Wc* AS A FUNCTION OF HELICAL PITCH (*P)* AND SPINDLE SPEED (*N)*. INTERPOLATION SPEED (F2) = 2.7 m/min, SHAFT LENGTH (L2) = 102 mm., C = C2.

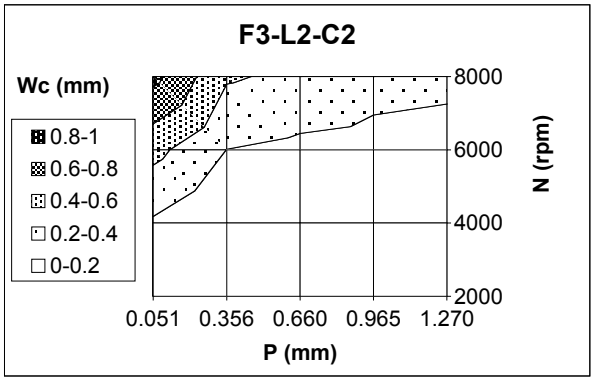

FIGURE 10. PROJECTED CHAMFER WIDTH *Wc* AS A FUNCTION OF HELICAL PITCH (*P)* AND SPINDLE SPEED (*N)*. INTERPOLATION SPEED (F3) = 5.0 m/min., SHAFT LENGTH (L2) = 102 mm, C = C2.

The photographs in Figure 8 show the extreme cases when chamfering is either too pronounced or too small, relative to the cross-hole dimensions (7.94 mm (5/16 in.) in diameter), and maximum burr root thickness of the samples (approx. 0.20 mm (0.008 in.)), respectively. The first case corresponds to the uppermost band of the *Wc* contour chart, where cutting conditions yield projected chamfer widths greater than 1.20 mm (0.047 in.). Although such overcut causes bore damage in the geometry tested, as shown in the top photograph, it should be noted that this is not the case in larger geometries with burr thicknesses approaching 1 mm. In the bottom photograph, the opposite scenario is evidenced. Chamfering is too small relative to burr root

thickness and the burrs remain on the edges. This case corresponds to the white area at the bottom of the chart. For the particular workpiece geometry tested, the chamfer width that guarantees burr removal with minimun overcut is 0.20 mm (0.008 in.). For any given workpiece geometry and drilling conditions, the optimum amount of chamfering depends on maximum burr root thickness.

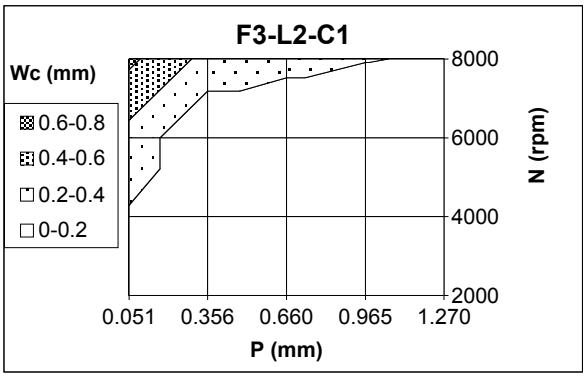

FIGURE 11. PROJECTED CHAMFER WIDTH *Wc* AS A FUNCTION OF HELICAL PITCH (*P)* AND SPINDLE SPEED (*N)*. INTERPOLATION SPEED (F3) = 5.0 m/min, SHAFT LENGTH (L2) = 102 mm., *C* = C1.

Figure 11 presents the *Wc* contour chart at fast feedrate F3, long tool shaft L2 and stiff coupling C2. A comparison of this chart with Figure 10 illustrates the effect of coupling type on chamfering efficiency. In essence, the stiff coupling removes more material than the compliant coupling under all testing conditions. With the compliant coupling, the "usable" area of the *Wc* contour chart is quite smaller and shifted towards the right, compared to the map from the stiff coupling. This means that to achieve the same chamfer width, smaller pitches, and thus longer cycle times, are required when using the compliant coupling. Indeed, at spindle speeds below 8000 rpm, the C2 coupling maximizes material removal.

The effect of shaft length was assessed as follows: in most cases, material removal increases slightly when shaft length is increased from 51 mm (2 in.) to 102 mm (4 in.) A comparison between the *Wc* maps in Figures 12 and 10 exemplifies the influence of shaft length on *Wc*. This result is particularly positive; it indicates that to reach intersections that are deep inside the workpiece, shaft length can be increased, to a certain extent, without undue reduction in chamfering performance.

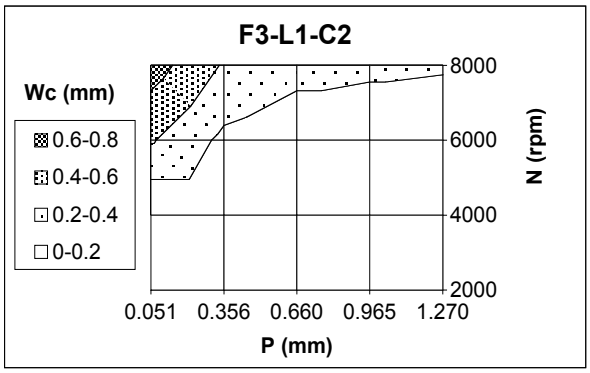

FIGURE 12. PROJECTED CHAMFER WIDTH *Wc* AS A FUNCTION OF HELICAL PITCH (*P)* AND SPINDLE SPEED (*N)*. INTERPOLATION SPEED (F3) = 5.0 m/min., SHAFT LENGTH (L1) = 51 mm, *C* = C2.

Marginal mean response graphs of *Wc*, with factors set at their lowest and highest values, are shown in Figure 13. The factors and 2-factor interactions with the greatest effect on *Wc* response (contrast) are clearly distinguished. In order of importance, these are: spindle speed

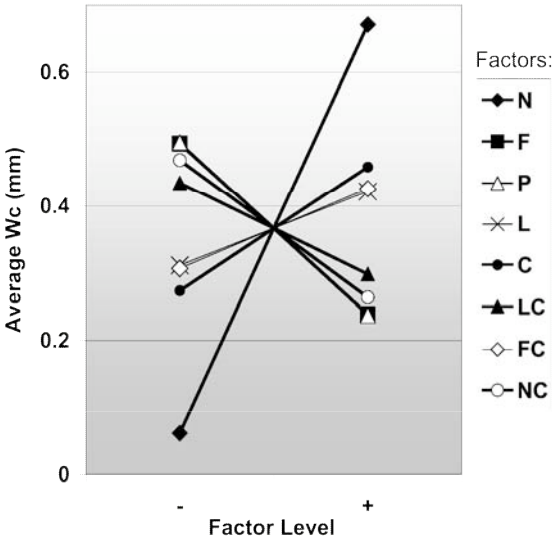

FIGURE 13. MARGINAL MEAN RESPONSE GRAPH OF PROJECTED CHAMFER WIDTH (*Wc*).

(*N*), helical pitch (*P*), feedrate (*F*), spindle speed-coupling type (*N*-*C*) interaction, coupling type (*C*), and shaft length-coupling type (*L*-*C*) interaction. It comes as no surprise that spindle speed is, by far, the control factor with the highest contrast. *Wc* response is also sensitive to helical pitch, because this factor determines the degree of overlap between tool passes along the hole intersection. Likewise, mean response is sensitive to feedrate when varied from F1 to F3. However, this response flattens considerably if levels are set at F2 and F3. Consequently, it is advised to adjust F, as opposed to P, to satisfy cycle time constraints. In contrast to the other main factors, it is verified that shaft length (*L*) has a relatively weak effect on *Wc*. Apart from *N*-*C* and *L*-*C*, it is found that 2-factor interactions have a weak effect on mean *Wc* response.

The contrast displayed by the *N*-*C* and *L*-*C* interactions can be further explored by studying their interaction graphs, which are shown in Figures 14 and 15, respectively. In Figure 14, it is observed that the increase in material removal as spindle speed increases, becomes

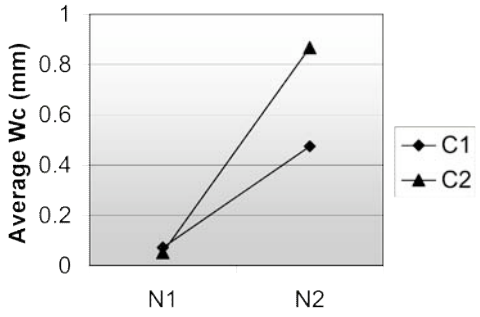

FIGURE 14. *N*-*C* INTERACTION GRAPH.

greater when the stiff coupling is used. On the other hand, the L-C interaction chart displays opposing slopes of the response curves. With the stiff coupling, an increase in shaft length enhances material removal, whereas with the compliant coupling, an increase in *L* slightly lowers material removal. Both behaviors derive from the dynamic effects of the mass of the coupling and the leverage provided by the shaft. The centrifugal force generated by the stiff coupling, which is almost twice as heavy as the compliant coupling, aids material removal. Ultimately, as spindle speed is increased, the chamfering enhancement produced by the stiff coupling stems from its mass, and not from its stiffness.

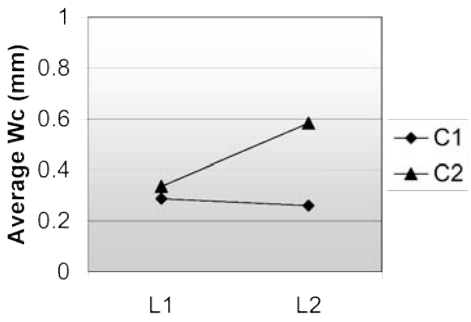

FIGURE 15. *L*-*C* INTERACTION GRAPH.

Figures 16 and 17 show the effect of cutting parameters on surface roughness R_t of the chamfered surfaces. Surface roughness increases monotonically with increasing spindle speed and helical pitch. On the other hand, roughness decreases slightly when interpolation speed is changed from 0.33 m/min (13 in./min) to 2.7 m/min (106 in./min), but then increases considerable at *F* = 5.0 m/min (198 in./min). This result should be taken into consideration whenever interpolation speeds need to be increased to reduce cycle times. A good compromise between surface quality and cycle time is achieved at a feedrate of 2.7 m/min.

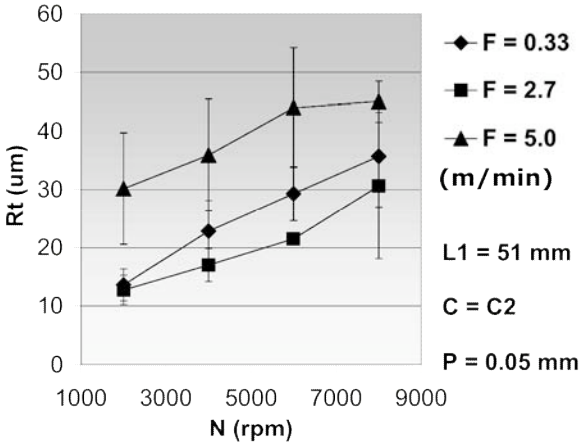

FIGURE 16. SURFACE ROUGHNESS R_t OF CHAMFERED EDGES AS A FUNCTION OF SPINDLE SPEED AND FEEDRATE. *L* = 51 mm, *C* = C2, *P* = 0.05 mm.

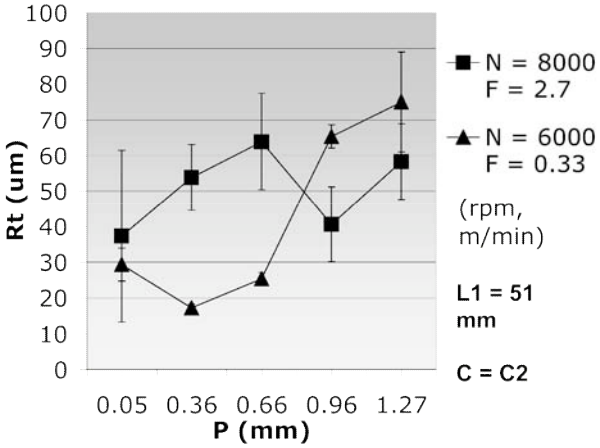

FIGURE 17. SURFACE ROUGHNESS R_t OF CHAMFERED EDGES AS A FUNCTION OF HELICAL PITCH. *L* = 51 mm., *C* = C2.

CONCLUSION

Experimental data of chamfer size and surface roughness were gathered to study the mechanized deburring process of cross-drilled intersections using the 6.35 mm (1/4 in.) Orbitool. Process maps for the selection of cutting conditions based on given burr root thickness and surface quality requirements were developed. The results are summarized as follows:

(1) Mechanized deburring with the Orbitool is a viable alternative to abrasive brush deburring. It offers improved control on chamfering, good consistency, and minimal bore surface damage. The technique is ideally suited for implementation in conventional machine tools, and does not contaminate the workpieces.

(2) Material removal at the hole intersection edges is mostly driven by rotational speed of the Orbitool, from 2000 to 8000 rpm, followed by helical pitch of the toolpath. The largest chamfers were obtained at 8000 rpm, however, the increase in chamfer size ceases asymptotically due to dynamic effects as spindle speed approaches 8000 rpm. Chamfering efficiency decreases with increasing helical pitch.

(3) Interpolation speed has a weak effect on material removal from 2.7 to 5.0 m/min. To satisfy cycle time constraints, it is recommended to adjust feedrate instead of helical pitch. It is also encouraged to attempt interpolation speeds above 5 m/min, since no large drops in chamfering efficiency are expected.

(4) The optimum chamfer size for a given deburring process is the minimum necessary for consistent burr removal, and it depends on the root thickness of the burrs.

(5) Dynamic effects of coupling mass influence material removal to a greater degree than static coupling stiffness. These effects enhance chamfering in the 2000 to 8000 rpm range, however, they become counterproductive above 8000 rpm. At such spindle speeds, elimination of the flexible coupling is recommended to reduce rotational mass.

(6) R_t roughness worsens with increasing spindle speed, helical pitch, and feedrate. Between feedrates of 0.33 and and 5.0 m/min, R_t reaches a minimum. Observed values were between 15 and 75 μm.

Cycle time of deburring operations performed in machine tools is particularly critical because the share of machine tool uptime for value-added operations must be maximized. To reduce operation time, testing of non-helical tool paths and interpolation speeds above 5 m/min are underway. Orbitools with less than 36 cutting edges are also tested to obtain higher material removal rates.

ACKNOWLEDGMENT

This research is supported by JWDone Company and the members of the Consortium on Deburring and Edge Finishing (CODEF).

REFERENCES

Dornfeld, D., Lisiewicz, V. (1992), “Acoustic Emission Feedback for Precision Deburring” *CIRP Annals*, Vol. 41, No. 1, pp. 93-96.

Fistere, Howard C. (1985), “Deburring Crossholes”, *Die Casting Engineer*, Vol. 29 No. 1, pp. 30-32.

Gillespie (1975), “Hand Deburring of Precision Miniature Parts”, *Bendix Aerospace, Kansas City Division Report* No BDX 613-1443.

Gillespie, L. K., (1990), “Deburring and Surface Finishing: The Past Ten Years and Projections for the Next Ten Years”, *Proc. Deburring Salon*, Burr, Edge, and Surface Technology, Japan, Japan Society of Precision Engineers, Nagoya, Japan.

Kim, J., Dornfeld, D., Furness, R. (1999), “Experimental Study of Burr Formation in Drilling of Intersecting Holes With Gun and Twist Drills”, *Tech Papers SME/NAMRI,* pp. 39-44.

Koelsh, J. R., (1990), “Banish Manual Deburring”, *Manufacturing Engineering*, Vol. 105 No. 1, pp. 71-75.

Ohshima, I., Maekawa, K., Murata, R. (1993), “Burr Formation and Deburring in Drilling Cross Holes”, *Journal of the Japan Society of Precision Engineering,* Seimitsu Kogaku Kaish*i*. Vol. 59 No. 1, January, pp.155-160.